

Fuel-Efficient Ship Routing

Kyriakos Avgouleas^a and Paul D. Sclavounos^b

^a*Lieutenant Commander HN, Submarine Shipbuilding Program, Hellenic Navy Detachment of Skaramangkas, Greece*

^b*Professor, Department of Mechanical Engineering, Massachusetts Institute of Technology, Cambridge MA, USA*

Abstract. Optimal weather routing of ships seeks to determine the voyage route, in rough seas, which minimizes a certain metric or criterion (e.g. transit time, consumed bunker fuel, pollutant emissions etc.). In this paper the problem of minimum-fuel navigation in a sea state is studied. Advanced methods of hydrodynamic simulation are employed to compute the added resistance in waves and the responses of an example-ship in random incident waves. A fictitious trans-Atlantic route is introduced. Given the wave forecast of the geographical region of interest, the problem of determining the route that minimizes fuel consumption is numerically solved using an improved Dynamic Programming algorithm. It is concluded that significant savings in bunker fuel may result from the implementation of a decision support system based on state-of-the-art hydrodynamics, wave forecasting and optimization methods.

Keywords: Routing; optimization; hydrodynamics; resistance; fuel consumption.

PACS: 02.30.Yy, 47.35.Lf

INTRODUCTION

The shipping industry consumes about 5% of the world oil production in bunker fuel for maritime transportation. That corresponds to approximately 4 million barrels of oil a day. This fact warrants an effort to optimize navigation in a way that will bring the fuel cost down to the extent possible. A new approach to the solution of the optimal routing problem is presented in this paper. A combination of frequency domain methods for the computation of the ship hydrodynamics, state-of-the-art weather forecasts and advanced dynamic programming algorithms is utilized to generate trajectories (ship routes in the ocean) which minimize the required fuel while meeting certain safety restrictions associated with the severity of the sea.

The optimization problem associated with the selection of the fuel-minimizing route of a ship in a sea state is challenging. In calm weather the optimal route within the constraints imposed by sea lanes is usually the loxodrome (or the orthodrome for long routes), and the fuel consumption is known with a high degree of certainty given the sailing distance and the calm water resistance and propulsion characteristics of the vessel. In rough weather a number of complexities arise. The severity of the sea states to be encountered during the trip is not known a priori with certainty and must be estimated from weather forecasts supplied by a routing service. When sailing in rough seas, safety criteria must be met that protect the integrity of the hull and the cargo. They affect the vessel speed and heading in a sea state. Reliable

seakeeping methods must be available in order to predict the vessel responses and the increase of her resistance in waves – the added resistance – given the attributes of the wave system. Finally, a robust and efficient dynamic optimization algorithm must be available that may be executed in real time to determine the optimal speed and heading of the vessel in rough weather in order to minimize the fuel consumption, subject to the safety constraints. These challenges are addressed in the present paper and an optimal ship routing algorithm is developed that leads to a notable reduction of the vessel fuel consumption in rough weather.

Literature Review

The problem of ship weather routing has been a subject of extensive research for many decades now. A comprehensive, albeit not exhaustive, review of the research work in the field starting from the 1950's can be found in Avgouleas (2008). Some of the developments in the last 10 years will be briefly presented here. Rathje and Beiersdorf (2005) developed a shipboard routing assistance (SRA) software to prevent containerships from encountering dangerous conditions with respect to seakeeping behavior (parametric rolling, slamming, exceedance of bending moment and shear force threshold values). Montes (2005) proposed a method for the automation of the Optimum Track Ship Routing (OTSR) system used by the US Navy. In Abramowski et al. (2006) a formal solution of the minimal time ship routing problem is presented on the basis of Pontryagin's maximum principle. Tsujimoto and Tanizawa (2006) solve the constrained optimization problem of minimum fuel routing, using the augmented Lagrange multiplier method. Böttner (2007) describes a decision support system able to provide optimal alternatives in case the ship finds herself in degraded condition (hull damage, rudder/propulsion failure etc.). The work of Szlapczyńska (2007) and extensions thereof (Szlapczyńska and Smierzchalski 2007-2009, Krata and Szlapczyńska 2011, Szlapczyńska 2013) focuses on deterministic weather routing of a sail assisted ship using Multi-Objective Evolutionary Algorithm (MOEA). Panigrahi et al. (2008) carry out a simulation of wave climate in the Indian Ocean and use it to minimize voyage time for a cargo ship route in the region. The optimization utilizes the Dijkstra algorithm and speed loss in waves is calculated from empirical curves. In Panigrahi et al. (2012) the hydrodynamics of ship motions and added resistance in waves are treated differently. Empirical speed loss curves are abandoned and standard frequency domain seakeeping computation is adopted. Sen and Padhy (2009) conducted a similar study using a Dijkstra algorithm as well, but with linear strip theory for hydrodynamic simulation. Wisniewski et al. (2009) utilize evolutionary algorithm to determine the minimum time route which safely avoids a tropical cyclone. Mezaoui et al. (2009) solve the unconstrained constant-speed minimum fuel problem in coastal navigation using high resolution forecasts and a Dijkstra optimization scheme. Dolinskaya et al. (2009) deduce shortest-time optimal paths inside convex regions of areas that a ship can sail. Their analysis is restricted to short-range optimal routing. Marie and Courteille (2009) deal with the deterministic dual-objective optimization of minimum time/minimum fuel route using Multi-Objective Genetic Algorithm (MOGA) and identifying Pareto optimal solutions. Hinnenthal and Clauss (2010) solve the same problem using similar principles but they quantify the robustness of the final solution exploiting ensemble forecasts. Delitala et al. (2010) explore the results of climatological simulations in combination with weather routing. Bruns et al. (2011) present a software tool for fuel efficient speed profile selection using potential flow CFD for calm water resistance prediction, strip theory for added resistance in waves and RANS modeling for the propulsor (both in design and off-design conditions). Gershanik (2011) addresses the challenges and benefits of weather routing optimization. The author advocates the use of the classical discrete dynamic programming algorithm (backward recurrence) for the minimum time or the minimum fuel optimal routing problem. Pipchenko (2011) solves the deterministic minimum work ship routing using genetic algorithm or a Nelder-

Mead heuristic method. Maki et al. (2011) propose a route optimization method that considers not only fuel efficiency but also ship stability (the risk of parametric rolling in particular). A real-coded genetic algorithm (GA) is used for the multi-objective optimization problem. Kobayashi et al. (2011) optimize the route of a containership in a simulated trans-oceanic passage, accounting for ship maneuvering dynamics. Dolinskaya (2012) introduces the notion of restricted turning radius in optimal path finding of a vessel in an inhomogeneous, non-stationary environment. Kosmas and Vlachos (2012) apply the simulated annealing method for the minimization of a cost function defined by the weighted sum of voyage time and a comfort parameter related to safety. Ilus and Heikkinen (2012) present a speed profile optimization approach which relies on historical and operational data collected for a specific route or leg of a voyage. The aim is to optimize energy usage while meeting prescribed constraints. Shao et al. (2012) solve the deterministic minimum fuel routing problem using a discrete 3D dynamic programming algorithm. Skoglund et al. (2012) present a method to obtain optimal routes in a directed graph using the concept of Pareto optimality. Both deterministic and ensemble forecasts are used. Tsou and Cheng (2013) combine an ant colony algorithm with a genetic algorithm for the solution of the minimal fuel and pollutant emission weather routing problem. In their recent work, Marie and Courteille (2014) construct a fuzzy logic model with data collected from ship's sensors to minimize fuel consumption of a sail-assisted motor vessel.

Model Overview

An example-ship is used from the Series 60 hullform, with the characteristics shown in table 1. A standard MARIN B-Series propeller is selected for this ship and a MAK 9M25C medium-speed, four-stroke diesel engine is matched with the propeller via a mechanical gearbox.

Resistance in calm water is calculated from standard statistical methods (Holtrop 1984). Added resistance in waves is computed using SWAN1, a frequency domain CFD code which uses 3D Rankine Panel Methods to simulate steady and unsteady potential flows around vessels with realistic hull shapes. Unlike most conventional strip and slender-body theories, SWAN1 exploits robust computational hydrodynamics methods to produce reliable results where approximate theories fail. The case of quartering and following waves can be mentioned as an example. At certain speeds they correspond to the sub-critical reduced frequency regime ($\tau < 1/4$) and represent challenging hydrodynamic problems intractable by strip theory. The same is true for the computation of added resistance in waves. Added resistance is a second order effect of central importance to weather routing, as it influences both the calculation of fuel consumption and the prediction of engine overload in a sea state. SWAN1 computes added resistance using direct integration and its results have been calibrated against numerous experiments carried out for America's Cup yachts (Sclavounos and Nakos 1993). In addition to resistance, all ship responses in waves are computed by SWAN1. In particular, pitch and heave motions and velocities near the ends of the hull are required to calculate probabilities of slamming and deck wetness. Limiting values imposed on these probabilities define safety constraints in the formulation of the minimum fuel consumption problem. Spectral analysis is used to estimate the mean added resistance and RMS values of the ship responses in a sea state with a given direction, significant wave height and modal period. The vessel hydrodynamic properties are computed a priori in the frequency domain across a wide range of encounter frequencies, ship speeds and wave headings and stored in a database for use in the solution of the fuel minimizing ship routing problem. Therefore, the time-consuming solution of the ship hydrodynamic problem in the time domain is avoided.

TABLE 1. Principal Dimensions of Example-Ship.

Description	Symbol	Unit	Value
Length at DWL	L	m	101.7
Beam at DWL	B	m	14.28
Draft at DWL	T	m	5.7
Freeboard at DWL (bow)	H	m	2.85
Displacement	Δ	<i>tonne</i>	5700
Wetted Surface Area	S	m^2	1950
Block Coefficient	C_B	-	0.676
Prismatic Coefficient	C_P	-	0.688
Midship Section Coefficient	C_M	-	0.982

TABLE 2. Propeller Characteristics of Example-Ship.

Description	Symbol	Value
Diameter (m)	D	3.2
Pitch Ratio	P/D	1.2
Expanded Area Ratio	EAR	0.75
Number of Blades	z	5

TABLE 3. Engine Characteristics of Example-Ship.

Description	Value
Type	MAK 9M25C
Rated Power (MCR) (kW)	3000
Rated Speed (rev/min)	750
Gear Ratio	4.45:1

A third generation model, WAM cycle 4, developed at the European Center for Medium-Range Weather Forecasts (ECMWF) and adapted by the University of Athens (UoA), Greece, provides the weather forecast for the region of interest. The forecast is uploaded daily and covers a total of 168 hours. A fictitious cross-Atlantic route starting from Cape St.Vincent, Portugal, and ending at Norfolk Virginia, USA, defines the nominal voyage track considered in the present study. It is assumed that the nominal (calm water) speed for this trip is 13 knots. The nominal sailing distance is 3138.6 nautical miles following the shortest route, which is the great circle route (orthodrome). At that speed the trip would last 10.06 days. Mercator projection is used throughout. For the part of the route not covered by the wave forecast, calm water is assumed.

Keeping the start and end points fixed (“hard” constraints) and the “expiration time” of the chartering contract also fixed (i.e. the time at destination), a special Dynamic Programming (DP) algorithm is implemented in MATLAB[®] which calculates the optimal route with backward

recurrence. To safeguard against the shortcomings of the standard DP algorithm, namely the large requirements for memory storage and processing capacity, Iterative Dynamic Programming (IDP) is employed. IDP is an advanced extension to the standard DP algorithm (Luus 2000). It retains all the benefits of DP without suffering the infamous drawback known as the “curse of dimensionality”.

HYDRODYNAMICS

Calm Water Resistance

Calm water resistance mainly consists of three components: friction, form and wave drag. The friction drag coefficient is calculated in this paper by the ITTC 1957 model-ship correlation line

$$C_f = \frac{0.075}{(\log_{10} Re - 2)^2} \quad (1)$$

The form drag coefficient is calculated from the Holtrop regression model (Holtrop 1984). It is given in the form of an enhancement factor k to the friction drag coefficient, based on the hull geometry and accounting for the presence of bilge keels (if present) and appendages. In this example, a bare Series 60 hull model is entered in the resistance calculations and the Holtrop resistance curve is shown in figure 1.

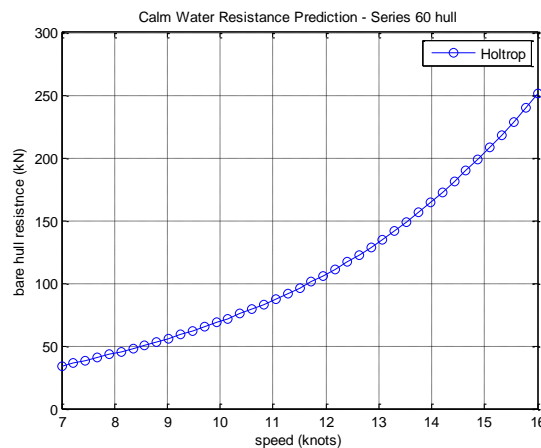


FIGURE 1. Steady Resistance from Holtrop Method.

The total calm water resistance coefficient is expressed as:

$$C_{total} = (1+k) \cdot C_f + C_w + C_a \quad (2)$$

where C_a is the model-ship correlation allowance and C_w the wave-making resistance coefficient, both obtained from the Holtrop statistical method. For a ship with total wetted surface S moving with constant forward speed U the total resistance is given by:

$$R_{calm} = C_{total} \cdot \frac{1}{2} \rho \cdot S \cdot U^2 \quad (3)$$

Propulsion

The thrust T and torque Q of a propeller with diameter D rotating at a speed n in a fluid with density ρ can be expressed in non-dimensional form as thrust and torque coefficients, K_T and K_Q respectively:

$$K_T = \frac{T}{\rho n^2 D^4} \quad (4)$$

$$K_Q = \frac{Q}{\rho n^2 D^5} \quad (5)$$

The speed at which the propeller is moving in the wake is the speed of advance U_A :

$$U_A = (1-w) \cdot U \quad (6)$$

The parameter w is an average measure of the wake effect and is termed *wake fraction*. The speed of advance can be non-dimensionalized to a parameter known as the advance ratio:

$$J = \frac{U_A}{nD} \quad (7)$$

The rate at which fuel mass is consumed in the engine is:

$$q = \text{sf}c(P_B) \cdot P_B \quad (8)$$

The engine break power P_B is related to resistance through the following expression:

$$P_B = \frac{R_{\text{total}} U}{\eta_D \eta_{TRM}} \quad (9)$$

The quasi-propulsive efficiency η_D can be expressed as the product:

$$\eta_D = \eta_R \eta_o \eta_H \quad (10)$$

The relative rotative efficiency η_R and hull efficiency η_H are parameters dependent mainly on the geometry of the hull. Although these parameters depend on speed too, the dependence on hull geometry dominates and they are often assumed constant in naval architecture. For the particular example-hull used here their values are 1.035 and 1.097 respectively, interpolated from the propulsion factors of the Series 60 parent models (Todd 1963). The open water propeller efficiency can be expressed in terms of the propeller parameters:

$$\eta_o = \frac{K_T J}{2\pi K_Q} \quad (11)$$

The term η_{TRM} in equation (9) stands for the transmission efficiency, which can be decomposed further into a product of shaft and gearbox efficiency:

$$\eta_{TRM} = \eta_S \eta_{GB} \quad (12)$$

In the example considered here the gearbox and shaft efficiencies are assigned typical values of 0.96 and 0.98 respectively.

Ship Dynamics in Waves

SWAN1 solves the linear forward speed seakeeping problem of the three-dimensional flow around vessels of arbitrary geometry. Linearity allows for the solution of the problem using frequency domain methods. The ambient waves are harmonic and so are the ship motions. Real sea states are modeled by spectral analysis using the frequency domain results from SWAN1. The computational domain for this study is shown in figure 2. The rectangular grid extends 50m from the bow to the upstream free surface boundary, 100m from the stern to the downstream boundary and 140m from the ship's centerline to the lateral boundary.

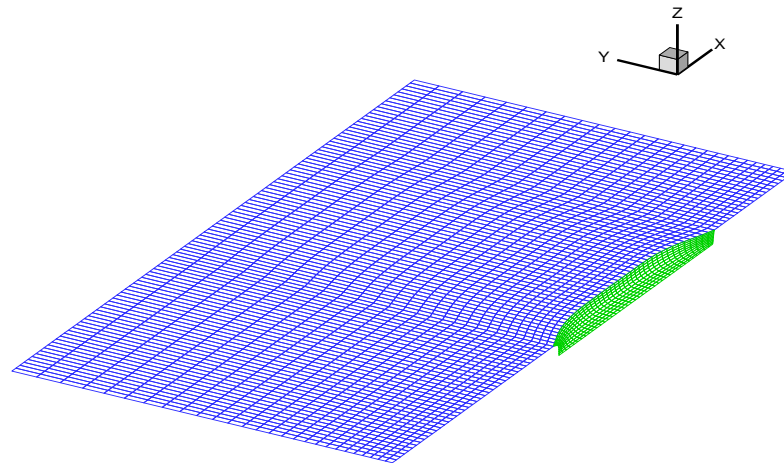


FIGURE 2. SWAN1 Computational Grid.

A ship-fixed reference frame $Oxyz$ with the $z=0$ plane coinciding with the calm water surface and the positive x -axis coinciding with the positive ship axis on the waterline is related to the earth-fixed $OXYZ$ frame through the Galilean transformation:

$$X = x + Ut \quad (13)$$

$$Y = y \quad (14)$$

$$Z = z \quad (15)$$

The total velocity potential $\Phi(\mathbf{x}, t)$ can be decomposed into a sum of two terms:

$$\Phi(\mathbf{x}, t) = \bar{\Phi}(\mathbf{x}, t) + \varphi(\mathbf{x}, t) \quad (16)$$

The first term on the right hand side represents the steady flow potential, which can be further decomposed into a basis flow and a disturbance flow:

$$\bar{\Phi}(\mathbf{x}, t) = \bar{\phi}(\mathbf{x}, t) + \psi(\mathbf{x}, t) \quad (17)$$

The basis flow potential $\bar{\phi}(\mathbf{x}, t)$ accounts for the thickness effect of the ship's hull as it

encounters the uniform ambient stream of velocity $-U$ (the moving ship is equivalently treated as fixed against an oncoming uniform flow). The disturbance potential $\psi(\mathbf{x}, t)$ accounts for the presence of the steady wave disturbance that forms the Kelvin wave pattern. The sum of these quantities satisfies the zero normal flux condition on the mean position of the hull. In SWAN1 the linearization of the steady flow is carried out around the double-body basis flow. The free surface is replaced by a rigid wall at $z=0$, on which:

$$\frac{\partial \bar{\phi}}{\partial z} = 0 \quad (18)$$

$\bar{\phi}(\mathbf{x}, t)$ represents the potential of the flow around the hull and its image above the plane $z=0$. By this representation, the hydrodynamic end effects are modeled more accurately than in typical strip and slender-body theories in which the basis flow is just the ambient free stream. The field equation, the free surface and radiation conditions and the aforementioned boundary conditions formulate a boundary value problem (BVP), which is solved numerically in SWAN1. The solution $\bar{\Phi}$ corresponds to a steady outgoing wave pattern known as the Kelvin wake.

The second term on the right hand side of (16) is the unsteady velocity potential associated with the ambient (harmonic) wave, its interaction with the hull and the resulting ship motions. It can be expressed as:

$$\varphi(\mathbf{x}, t) = \Re e \left\{ \tilde{\varphi}(\mathbf{x}) e^{i\omega t} \right\} \quad (19)$$

In the above expression the harmonic term oscillates with the encounter frequency ω :

$$\omega = |\omega_o - kU \cos \beta| \quad (20)$$

where ω_o is the absolute ambient wave frequency defined relative to the earth fixed coordinate system and k the corresponding wavenumber, given by the dispersion relation in deep water:

$$k = \frac{\omega_o^2}{g} \quad (21)$$

Following the standard convention for relative wave direction, the angle β is measured from the stern ($\beta=180^\circ$ means head wave).

The complex potential $\tilde{\varphi}$ in (19) is a superposition of the incident wave potential $\tilde{\varphi}_I$, the diffraction potential $\tilde{\varphi}_D$ and the radiation potentials $\tilde{\varphi}_j$, $j=1, \dots, 6$ for all modes of motion:

$$\tilde{\varphi} = \tilde{\varphi}_I + \tilde{\varphi}_D + \sum_{j=1}^6 \tilde{\varphi}_j \quad (22)$$

SWAN1 solves the relevant BVP for the diffraction potential $\tilde{\varphi}_D$ and calculates the (complex) excitation forces from the linearized Bernoulli equation extended to account for the modeling of end effects by the double-body basis flow:

$$\tilde{P} = -\rho \left(i\omega - U \frac{\partial}{\partial x} \right) \cdot (\tilde{\varphi}_I + \tilde{\varphi}_D) \quad (23)$$

$$\tilde{X}_i = \iint_{S_B} \tilde{P}n_i dS \quad (24)$$

Furthermore, upon solving the BVP for the radiation potentials $\tilde{\phi}_j$ SWAN1 provides the complex amplitudes of motion for all six degrees of freedom in the form of Response Amplitude Operators (RAO), normalized by the ambient wave amplitude:

$$RAO_j(\omega) = \frac{\Xi_j(\omega)}{A}, \quad j=1, \dots, 6 \quad (25)$$

Examples of RAOs in heave and pitch in oblique (bow and stern quartering) waves for a Froude number of 0.21 (13 knots) are shown in figures 3 to 6. The RAO's are plotted against the encounter period of the wave.

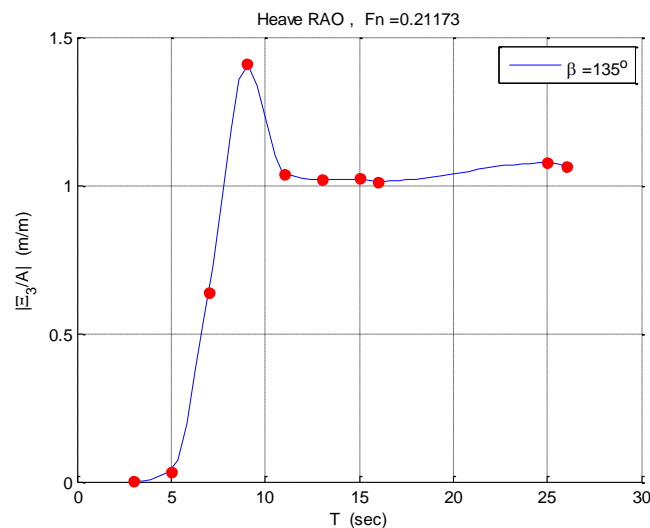


FIGURE 3. Heave RAO in Bow Waves at 13 Knots.

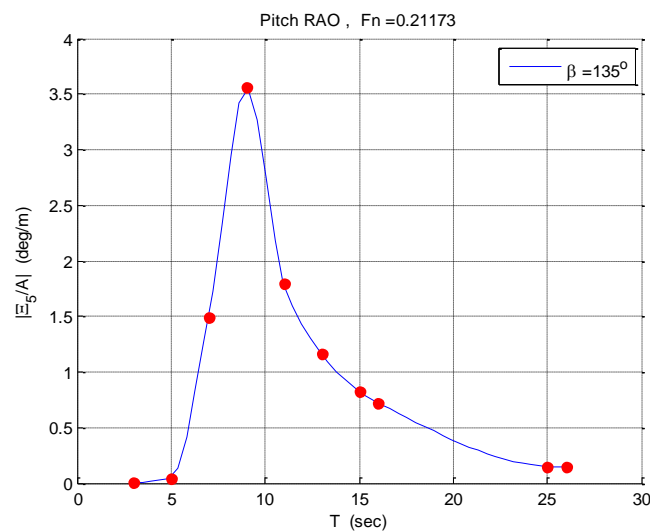


FIGURE 4. Pitch RAO in Bow Waves at 13 Knots.

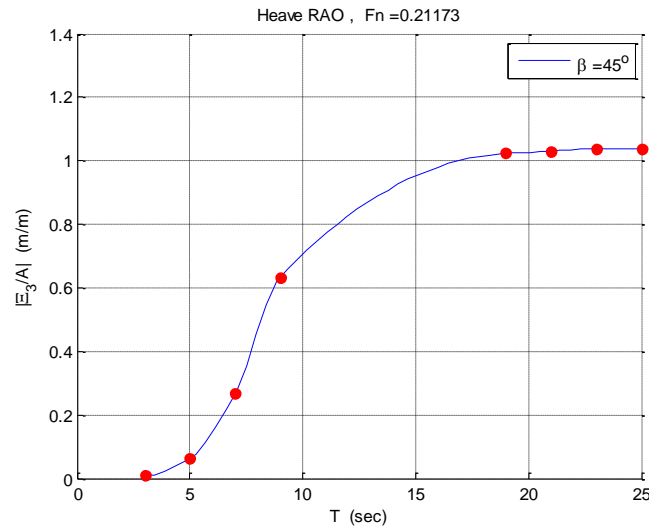


FIGURE 5. Heave RAO in Quartering Waves at 13 Knots.

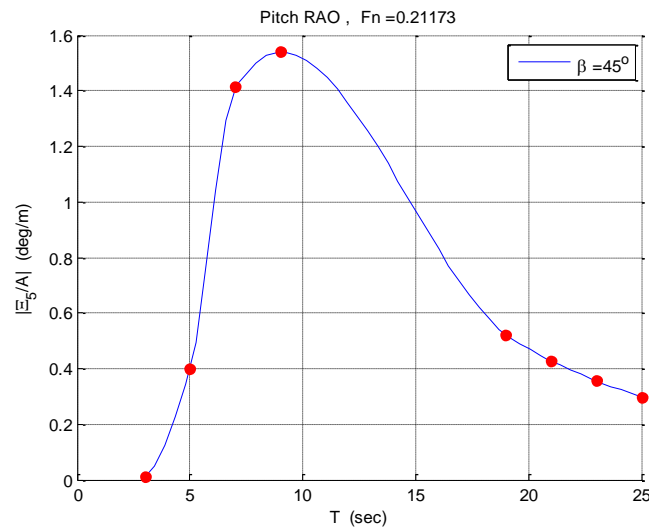


FIGURE 6. Pitch RAO in Quartering Waves at 13 Knots.

Added Resistance in Waves

Added resistance is a hydrodynamic force of paramount significance to the ship routing problem. The effect of waves manifests itself in the fuel consumption through the existence of this additive resistance force. Standard methods exist for the calculation of added resistance, but with relatively narrow range of applicability in terms of wave direction (Gerritsma and Beukelman 1972) or Froude numbers (Faltinsen et al. 1980).

SWAN1 implements the direct pressure integration method and accurately models the hydrodynamic effects near the ends of the ship which are essential for the robust prediction of the added resistance. The total velocity potential is given by (16). The total resistance is the x-component of the hydrodynamic force:

$$R_T = - \iint_{S_B} P n_1 dS_B \quad (26)$$

The above force is obtained by integrating the total hydrodynamic pressure:

$$P = -\rho \left(\frac{\partial \Phi}{\partial t} + \frac{1}{2} \nabla \Phi \cdot \nabla \Phi + gz \right) \quad (27)$$

around the instantaneous submerged hull surface S_B . Replacing Φ by the steady flow potential $\bar{\Phi}$ in (27) and integrating the resulting \bar{P} over the mean surface of the submerged hull, the calm water resistance follows:

$$R_{calm} = - \iint_{\bar{S}_B} \bar{P} \bar{n}_1 dS_B \quad (28)$$

The difference between the total and calm water resistance is oscillatory, time dependent and can be written as the sum of three components:

$$R_{total} - R_{calm} = R_1 + R_2 + R_3 \quad (29)$$

$$R_1 = - \iint_{\bar{S}_B} \delta P \bar{n}_1 dS_B \quad (30)$$

$$R_2 = - \iint_{\bar{S}_B} \bar{P} \delta n_1 dS_B \quad (31)$$

$$R_3 = - \iint_{\delta S_B} \bar{P} \bar{n}_1 dS_B \quad (32)$$

In the above relations, δS_B represents the fluctuation of the mean wetted surface \bar{S}_B that accounts for the ship motions, δP is the correction to the steady pressure P at some rigid point on the instantaneous position of the hull in waves and δn_1 is the difference between the x-component of the unit normal vector at the instantaneous and mean positions of the hull. By expanding (29) in a Taylor series around the mean position of the hull, the quantities δS_B , δP , δn_1 appear explicitly in terms of $\bar{\Phi}$, φ and their gradients evaluated at the mean positions of the hull and the waterline. Since the latter quantities are available from the solution of the linear seakeeping problem, the added resistance can be calculated. For a monochromatic wave of amplitude A and frequency ω , at an angle of incidence β the added resistance is defined as the mean of (29), namely:

$$R_w(\omega, \beta) = \overline{R_1 + R_2 + R_3} \quad (33)$$

In SWAN1 the output is expressed as an Added Resistance Operator (ARO) normalized by the square of the ambient wave amplitude:

$$ARO(\omega, \beta) = \frac{R_w(\omega, \beta)}{A^2} \tag{34}$$

Figures 7, 8 plot ARO vs. encounter period for the same wave headings as in figures 3 to 6.

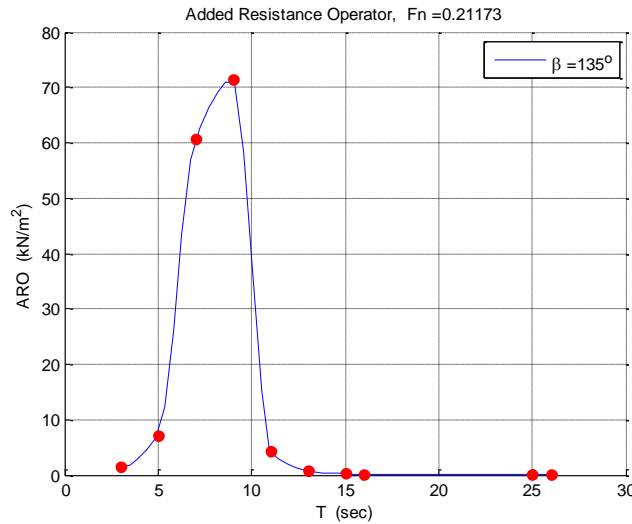


FIGURE 7. Added Resistance Operator in Bow Waves at 13 Knots.

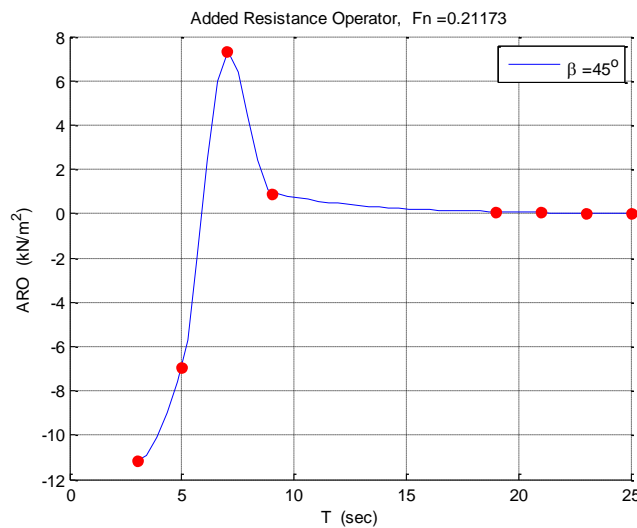


FIGURE 8. Added Resistance Operator in Quartering Waves at 13 Knots.

For irregular seas characterized by a spectrum $S(\omega_0, \theta)$ the mean added resistance can be found by integrating the ARO and the spectral density over all constituent absolute wave frequencies and headings:

$$\bar{R}_w = 2 \int_0^\infty d\omega_0 \int_{-\frac{\pi}{2}}^{\frac{\pi}{2}} d\theta S(\omega_0, \theta) \cdot ARO[\omega(\omega_0), \theta] \tag{35}$$

As explained below, wave and swell are treated as locally unidirectional, propagating along the mean directions computed by the forecasting model. In this setting integration over θ in (35) need not be carried out. In the evaluation of the mean added resistance by (35) the dependence of the ARO on the encounter frequency defined by (20) has been used to transform the integration in (35) over the absolute wave frequency.

SEA STATE MODELING AND FORECASTING

By means of an advanced CFD tool like SWAN1, the ship hydrodynamics in calm water and in waves is properly modeled, as outlined in the preceding section. In addition to resistance and powering, predicting the variability of the ocean environment is a necessity in optimal ship navigation. In this paper the representation of the sea state is derived from the results of the ECMWF global version of the WAM numerical model. The model solves the wave transport equation (i.e. the governing law of wind-wave energy balance) without any assumption on the spectral shape. The solution is the spectral density given at 28 different frequencies and 24 wave directions for every grid point on the global map (Emmanouil et al. 2007). After processing the spectral information, the output contains significant wave height, maximum expected wave height, mean and peak frequencies and mean wave direction. For swell waves the output provides swell height, mean direction and mean frequency. These results constitute the wave and swell forecasts which are promulgated daily in 1-hour time intervals at each grid point. For reasons of computational efficiency the study presented here makes use of the forecast data in 3-hour time steps. The spatial resolution of 0.5×0.5 degrees corresponds to an area of roughly 55×55 km.

Although WAM4 calculates the spectrum, the enormous size of the data files makes it impossible to process the direct information of spectral density $S(\phi, \lambda, \omega, \theta, t)$ as a function of position (i.e. longitude λ -latitude ϕ), frequency ω , direction θ and time t . Practical considerations, therefore, dictate the need to back-fit the output parameters of the model (namely mean frequency and wave height) to a standard spectrum which is anticipated to represent the actual sea state reasonably well. A bi-modal Bretschneider spectrum is selected for this purpose. By virtue of linearity, two separate single-peaked Bretschneider spectra can be superimposed, one describing the local storm (i.e. wind-generated waves) the other describing the swell. The expression for each of them is:

$$S(\omega) = 0.278 \frac{\bar{\omega}^4}{\omega^5} \bar{H}^2 e^{-0.437(\bar{\omega}/\omega)^4} \quad (36)$$

where $\bar{\omega}$ and \bar{H} stand for the mean frequency and height of the wave (or swell) respectively. \bar{H} is related to the significant wave height H_s via:

$$\frac{H_s}{\bar{H}} = 1.6 \quad (37)$$

The forecast time interval of 3 hours corresponds to a time window for which the assumption of stationarity of the sea state holds well. Stationarity, in turn, permits the utilization of frequency domain methods and spectral analysis in hydrodynamics which together with linearity allow the calculation of the mean added resistance from expression (35) and the estimation of the ship response statistics from analogous expressions. For example, the variance of heave motion (mode 3 in SWAN1) can be easily calculated, given the wave

spectrum and the RAO in heave:

$$\sigma_3^2 = \int_0^{\infty} S(\omega_o) |RAO_3(\omega_o)|^2 d\omega_o \quad (38)$$

The variances of other derived responses may be evaluated in a similar manner and used in the equations of the constraints in the optimal control problem in question.

All hydrodynamic attributes of a particular vessel of interest in the minimum fuel routing problem are contained in the ship response RAOs and the added resistance ARO. These quantities are computed once, in advance, as functions over all absolute wave frequencies, ship speeds and headings in unidirectional waves and stored in a hydrodynamic database customized for each vessel. They are subsequently used in expressions (35) and (38) together with the wave spectra supplied by the weather forecasts. As will be seen below the mean added resistance and RMS values of the ship responses are the quantities that enter the minimum fuel routing problem and their evaluation is very efficient given the ARO and RAOs which are retrieved from the hydrodynamic database.

Treating the spectrum as locally unidirectional in the vicinity of each position on the map (grid point \mathbf{x}), the variance in equation (38) and the added resistance in (35) are both functions of the local prevailing direction of propagation θ_0 of the sea state (i.e. the mean direction). Technically, the local directionality of the sea state is modeled by multiplying the spectral density by a “spreading function”, which in this setting is a delta function located at θ_0 :

$$S(\omega_o, \theta) = \delta(\theta - \theta_0) \cdot S(\omega_o) \quad (39)$$

Integration of an expression like (35) over all angles with the spectrum cast in the form of (39) eliminates all but one direction θ_0 . If the assumption of long-crested waves propagating in one direction is lifted, some directional spreading should be included in the model at the higher computational cost incurred by the double integration in (35). The use of different spreading functions (i.e. delta, $\cos^2()$, $\cosh^{-2}()$, Hasselmann formula, Mitsuyasu formula etc.) and their effect on the optimal solution and computational time will be addressed in future work.

MINIMUM FUEL ROUTING

Powering and Fuel Consumption in Rough Seas

The equations of motion of the ship sailing in the ocean can be written in spherical coordinates as:

$$\dot{\phi}(t) = \frac{1}{R_{earth}} \cdot U(t) \cdot \cos(p(t)) \quad (40)$$

$$\dot{\lambda}(t) = \frac{1}{R_{earth} \cdot \cos(\phi(t))} \cdot U(t) \cdot \sin(p(t)) \quad (41)$$

The speed of the vessel is denoted by U and the course is denoted by p (measured relative to the true north). U refers to the speed through water (STW), which in the absence of currents coincides with the speed over ground (SOG). The latter is accurately measured by the GPS receivers on board. Ocean currents are not considered in the present study, but their inclusion in the model is straightforward. The spherical coordinates in the above equations are the latitude

$\phi \in \left(-\frac{\pi}{2}, \frac{\pi}{2}\right)$, measured from the equator (positive north), and the longitude $\lambda \in (-\pi, \pi]$ measured from the Greenwich meridian (increasing eastbound). \bar{R}_{earth} is the mean radius of the earth. The differential distance between positions (ϕ, λ) and $(\phi + d\phi, \lambda + d\lambda)$, if measured along the rhumb line (loxodrome) connecting the two locations, is given by:

$$dS = U(t) \cdot dt = \bar{R}_{earth} \cdot \sqrt{d\phi(t)^2 + \cos^2(\phi(t)) \cdot d\lambda(t)^2} \tag{42}$$

The loxodrome is the constant heading route connecting any two locations on the sphere. On a Mercator map this route appears as a straight line. On the other hand, the shortest distance between two points on the sphere is obtained if these two points are connected with a great circle arc. This is the orthodrome route. The great circle distance between points (ϕ_1, λ_1) and (ϕ_2, λ_2) is:

$$S = \bar{R}_{earth} \cdot \cos^{-1}(\sin(\phi_1)\sin(\phi_2) + \cos(\phi_1)\cos(\phi_2)\cos(\lambda_2 - \lambda_1)) \tag{43}$$

It is customary in navigation to approximate the great circle route with a sequence of rhumb line segments. This is the approach adopted throughout this paper.

The position vector $\mathbf{x}(t) = (\phi(t) \ \lambda(t))^T$ is the state vector of the system, while $\mathbf{u}(t) = (U(t) \ p(t))^T$ is the control vector. Assuming quasi-steady conditions, the thrust delivered by the propulsor is balanced by the total resistance:

$$T(U, p, \phi, \lambda, \tilde{t}) = \frac{R_{calm}(U) + \bar{R}_w(U, p, \phi, \lambda, \tilde{t})}{1-t} \tag{44}$$

where \tilde{t} denotes time to distinguish it from the thrust deduction factor defined as $t = \frac{T-R}{T}$. Combining equations (4), (6), (7) and (44) yields the propeller load curve:

$$K_T = \frac{R_{calm}(U) + \bar{R}_w(\mathbf{u}, \mathbf{x}, \tilde{t})}{\rho(1-t)(1-w)^2 U^2 D^2} J^2 \tag{45}$$

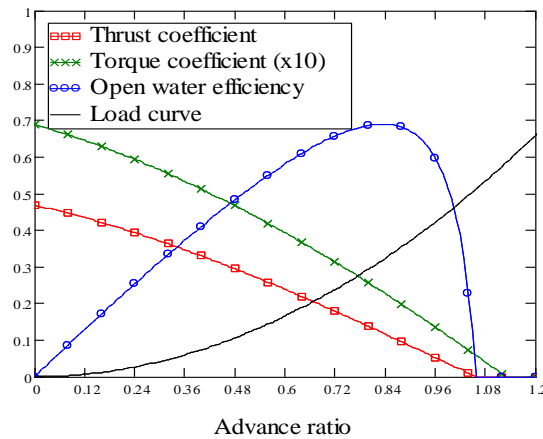


FIGURE 9. Typical B-Series Chart. Intersection of load curve with thrust coefficient curve uniquely defines all the operational parameters of the propeller.

Equation (45) together with the K_T curve of the B-series chart define a nonlinear system of equations for the unknowns K_T and J . Upon solving this system, the parameters K_Q and η_o are readily calculated from (5) and (11) respectively. Figure 9 shows a graphical solution on the chart. The point of intersection of the load curve with the thrust coefficient curve uniquely determines the advance ratio J , from which the corresponding K_Q and η_o can be read off the chart. From equations (8)-(12), the fuel rate can be expressed formally as a function of position in the ocean, control setting (i.e. speed and course) and time:

$$q(\mathbf{u}, \mathbf{x}, \tilde{t}) = sfc \cdot \frac{R_{calm}(U) + \bar{R}_w(\mathbf{u}, \mathbf{x}, \tilde{t})}{\eta_R \cdot \eta_o(\mathbf{u}, \mathbf{x}, \tilde{t}) \cdot \eta_H \cdot \eta_S \cdot \eta_{GB}} \cdot U \quad (46)$$

The product of the last two terms in (46) is the engine load (break power). The dependence of the term sfc on engine load has been suppressed for brevity. Figure 10 demonstrates this dependence for the MAK 9M25C engine.

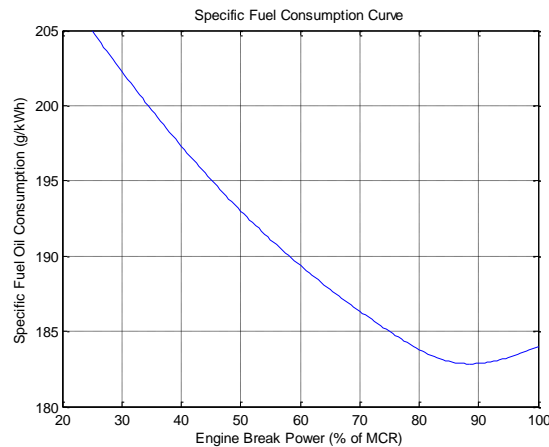


FIGURE 10. Specific Fuel Consumption as a Function of Engine Load (data source: ref [22]).

The integral of (46) over the entire duration of the trip defines a scalar performance index:

$$I = \int_0^{t_f} sfc \cdot \frac{R_{calm}(U) + \bar{R}_w(\mathbf{u}, \mathbf{x}, \tilde{t})}{\eta_R \cdot \eta_o(\mathbf{u}, \mathbf{x}, \tilde{t}) \cdot \eta_H \cdot \eta_S \cdot \eta_{GB}} \cdot U d\tilde{t} \quad (47)$$

The above index quantifies the total amount of fuel which has been consumed upon reaching the fixed final time t_f . It is the cost function to be minimized in the optimization process.

Inequality Constraints

While seeking to minimize (47) there are certain limiting factors which in a typical optimal control problem appear as inequality constraints. Violation of these constraints is prohibited at all times and this restriction changes the structure of the solution.

State Constraints, namely limits in ϕ and λ , could represent regions of forbidden navigation, such as shallow waters, land or ice. The numerical simulation in this study was carried out in the Atlantic Ocean below the arctic circle, so the possible influence of shallow waters and ice is not investigated.

Control Constraints are bounds imposed by the propulsion plant capabilities. For example, the particular ship cannot exceed 15.45 knots in calm seas with the given engine at the particular loading condition, assuming clean hull. In addition, the engine load (an implicit function of the controls) is not permitted to exceed an envelope function $g(P_B, n_e)$ which is depicted in figure 11, otherwise the engine will be overloaded. P_B and n_e represent the engine load and speed respectively.

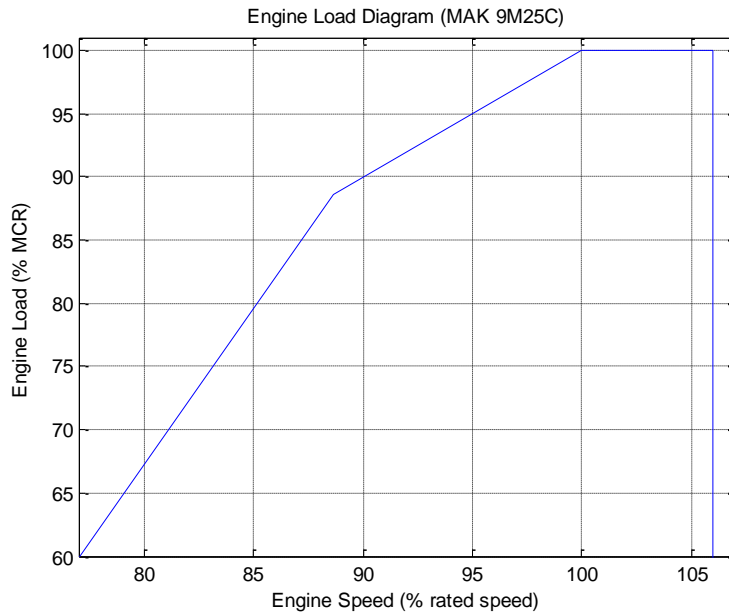


FIGURE 11. Engine Operating Envelope (data source: ref. [22]).

Therefore, the control bounds can be described as follows:

$$P_B(U, p) \leq g(P_B, n_e) \quad (48)$$

$$U_{\min} \leq U \leq U_{\max} \quad (49)$$

In principle, the lower bound for speed should be zero. However, in the optimization example described below it was found that there is no gain in lowering the speed below 7 knots. As verified by SWAN, the responses in speeds lower than 7 are practically those of the ship at zero speed. Regardless of the initial conditions or the trial forecasts, it was observed that the program would always choose to avoid severe weather by altering the ship's course while retaining speed above 7. Furthermore, there exists a lower bound for engine speed to avoid excessive vibrations. In order to save computational effort the lower bound U_{\min} was set to 7 knots. This limit corresponds (in calm water) to an engine speed of 311 revs/min, well above the minimum allowable speed of 250 revs/min for this particular engine type (ref. [22]).

Safety Constraints are enforced to ensure the secure transportation of the cargo and the physical integrity of the ship herself, while moving in rough seas. Quantifying safety is not a trivial task. The approach proposed here is to enforce “hard” inequality constraints on the probabilities of occurrence of certain extreme events associated with sea severity. Two such events are green water on deck (or deck wetness) and slamming. Other motion-related constraints could also be specified, at increased computational cost, depending on the type of vessel and nature of risks that must be taken into account when sailing in severe weather. For instance, parametric rolling is a dangerous situation that should be avoided especially in container transportation. In what follows, only restrictions on deck wetness and slamming have been considered, as they are deemed sufficient to demonstrate the concept and the benefits of constrained optimal routing. It should be noted that these two events are related to pitching and heaving, two longitudinal modes of ship motion which can be predicted by SWAN1 with remarkable accuracy. Considering a point Π_1 in the uppermost part of the bow (bulwark), deck wetness occurs when the relative motion exceeds the freeboard f at point Π_1 . The probability of this event follows the Rayleigh distribution (Ochi 1998) and is given by:

$$P(\text{water on deck}) = e^{-\frac{f^2}{2\sigma_r^2}} \quad (50)$$

The variance of the relative motion, σ_r^2 , is calculated by an expression similar to (38). Slamming occurs when the relative motion at a point Π_2 in the keel near the bow exceeds the draft H at that point and when the relative velocity exceeds a critical value:

$$V_{cr} = 0.093\sqrt{g \cdot L} \quad (51)$$

The critical velocity V_{cr} , gravitational acceleration g and waterline length L enter equation (51) in SI units. Assuming that the two events are statistically independent, the probability of slamming follows the Rayleigh distribution:

$$P(\text{slamming}) = e^{-\left(\frac{H^2}{2\sigma_r^2} + \frac{V_{cr}^2}{2\sigma_v^2}\right)} \quad (52)$$

where σ_r^2 and σ_v^2 are the variances of the relative motion and velocity, respectively, at point Π_2 .

When the frequency of occurrence of slamming or deck wetness rises above certain limits, the motions are so severe that the ship’s safety is compromised and voluntary speed reduction is effected. The limiting probabilities assume the following values (Faltinsen 1990):

$$P(\text{slamming}) \leq 0.03 \quad (53)$$

$$P(\text{water on deck}) \leq 0.07 \quad (54)$$

Substituting (50) and (52) in (53) and (54), respectively, and taking the logarithms of both sides the safety constraints take the form of inequalities involving the RMS values of the relative motion and velocities at selected points on the hull. The RMS values of these and other derivative seakeeping quantities may be evaluated easily from their definition and the use of expressions analogous to (38).

Formulation of the Optimal Routing Problem

The complete formulation can be summarized in the standard format for constrained optimization problems:

$$\text{minimize } I = \int_0^{t_f} sfc \cdot \frac{R_{calm}(U) + \bar{R}_w(\mathbf{u}, \mathbf{x}, \tilde{t})}{\eta_R \cdot \eta_o(\mathbf{u}, \mathbf{x}, \tilde{t}) \cdot \eta_H \cdot \eta_S \cdot \eta_{GB}} \cdot U d\tilde{t}$$

subject to:

Dynamic constraint:

$$\dot{\phi}(t) = \frac{1}{\bar{R}_{earth}} \cdot U(t) \cdot \cos(p(t))$$

$$\dot{\lambda}(t) = \frac{1}{\bar{R}_{earth} \cdot \cos(\phi(t))} \cdot U(t) \cdot \sin(p(t))$$

Control bounds:

$$P_B(U, p) \leq g(P_B, n_e)$$

$$U_{\min} \leq U \leq U_{\max}$$

Safety constraints:

$$P(\text{slamming}) = e^{-\left(\frac{H^2}{2\sigma_r^2} + \frac{V_{cr}^2}{2\sigma_v^2}\right)} \leq 0.03$$

$$P(\text{water on deck}) = e^{-\frac{f^2}{2\sigma_r^2}} \leq 0.07$$

initial and terminal conditions:

$$\mathbf{x}(0) = \begin{pmatrix} \phi(0) \\ \lambda(0) \end{pmatrix} = \begin{pmatrix} \phi_0 \\ \lambda_0 \end{pmatrix}$$

$$\mathbf{x}(t_f) = \begin{pmatrix} \phi(t_f) \\ \lambda(t_f) \end{pmatrix} = \begin{pmatrix} \phi_f \\ \lambda_f \end{pmatrix}$$

and final time:

t_f prescribed

In order to solve the problem numerically the discrete counterparts of the cost function and

dynamic constraint are needed. The sailing time is divided into N stages of length:

$$\Delta t = \frac{t_f}{N} \quad (55)$$

The equations of motion are approximated as:

$$\phi(k+1) = \phi(k) + \frac{1}{R_{earth}} \Delta t U(k) \cos p(k) \quad (56)$$

$$\lambda(k+1) = \lambda(k) + \frac{1}{R_{earth} \cdot \cos(\phi(k))} \Delta t U(k) \sin p(k) \quad (57)$$

with $\phi(1) = \phi_0$, $\lambda(1) = \lambda_0$, $\phi(N+1) = \phi_f$, $\lambda(N+1) = \lambda_f$ and $k = 1, 2, \dots, N$.

The integrand in (47) is the Lagrangian. In discrete form the integral is approximated by a sum and the performance index becomes:

$$I = \sum_{k=1}^N q(U(k), p(k), \phi(k), \lambda(k), k) \Delta t \quad (58)$$

NUMERICAL SOLUTION

Dynamic Programming

Dynamic Programming (DP) was introduced by Richard Bellman in the 50's and has proven to be an invaluable tool in optimal control, especially for problems that do not admit an analytical solution. Many such problems do not satisfy optimality or existence and uniqueness conditions. In these cases the classical calculus of variations formulation falls short. Yet, these problems may possess an optimal solution which can be found by DP. Mathematical principles of the method can be found in Bellman (1957). A standard DP algorithm is presented in Kirk (1970).

Iterative Dynamic Programming (IDP) is a recent evolution of the same idea. It applies the recurrence relation known as the Bellman equation in an iterative fashion, converging to the solution in each iteration. The IDP algorithm can be implemented with surprisingly few grid points, thus eliminating the most prominent weakness of the standard DP algorithm: as the number of dimensions grows the vast size of memory storage becomes prohibitive. In fact, the IDP version adopted in this paper uses only a single grid-point. The algorithm outlined below in 10 steps, is adapted by Luus (2000):

1. Discretize the time interval $[0, t_f]$ into N time stages of equal length Δt . Δt should be chosen to coincide with the forecast interval. If $t_f \neq N \cdot \Delta t$, an additional time stage is required of length

$$\Delta t' = t_f - N \cdot \Delta t.$$

2. Make an initial "guess" for the entire control sequence $\mathbf{u}^*(k)$ ($k = 1, \dots, N$). In the iteration following the first, this will be the optimal control obtained in the previous iteration. Using $\mathbf{u}^*(k)$

integrate (40)-(41) to generate an initial nominal trajectory $\mathbf{x}^*(k)$, where $k=1, \dots, N+1$. Alternatively, one can “guess” the nominal trajectory $\mathbf{x}^*(k)$ and compute the corresponding initial control history $\mathbf{u}^*(k)$.

3. Choose the number of controls c_r ($r=1, 2, \dots, m$) for each element of the $m \times 1$ control vector \mathbf{u} . The total number of controls is $C = c_1 \cdot c_2 \cdot \dots \cdot c_m$. Choose the control region contraction factor γ .
4. Choose an increment $\Delta \mathbf{u}$ that determines the span of control region around the central value \mathbf{u}^* , i.e.

$${}^j \mathbf{u}^* \pm \Delta \mathbf{u} \cdot {}^j R \quad (59)$$

The left superscript j denotes iteration number. The quantity ${}^j R$ is a scaling factor applied to $\Delta \mathbf{u}$. It is responsible for narrowing the control region around ${}^j \mathbf{u}^*$ in every iteration. For the first iteration ${}^1 R = 1$.

5. Discretize each element r of $\Delta \mathbf{u}$ into $\frac{c_r}{2}$ quantized values. These values are selected randomly in the range $\Delta \mathbf{u}$.
6. Start the iterations by setting $j=1$, ${}^j R = 1$.
7. Move two steps back from the terminal state to the beginning of stage $N-1$. This corresponds to time $t_f - 2\Delta t$. Integrate forward along the next stage, that is from time $t_f - 2\Delta t$ to time $t_f - \Delta t$, C times using C different values of \mathbf{u} :

$$\mathbf{u}(N-1) = {}^j \mathbf{u}^*(N-1) \pm \Delta \mathbf{u} \cdot {}^j R \quad (60)$$

If any of the elements of $\mathbf{u}(N-1)$ falls outside the allowable values for control, clip them at the upper or lower bound as appropriate. The integration starts from the known state ${}^j \mathbf{x}^*(N-1)$ of the current optimal path. Calculate the reached state $\mathbf{x}^r(N)$ ($r=1, 2, \dots, C$) and integrate along the final stage to close in on the (fixed) destination point (i.e. the terminal state). Calculate the associated performance index I for each of the C different controls for this two-leg route. Find the r for which I is minimized and store the corresponding $\mathbf{u}^r(N-1)$ as ${}^{j+1} \mathbf{u}^*(N-1)$.

8. Move one step further back, to the beginning of stage $N-2$ (corresponding to time $t_f - 3\Delta t$). Starting from state ${}^j \mathbf{x}^*(N-2)$ integrate one step forward, up to time $t_f - 2\Delta t$, using C different values of \mathbf{u} :

$$\mathbf{u}(N-2) = {}^j \mathbf{u}^*(N-2) \pm \Delta \mathbf{u} \cdot {}^j R \quad (61)$$

Calculate the reached state $\mathbf{x}^r(N-1)$. For every r , carry out the integration of the remaining trajectory up to the terminal state. Use the optimal control ${}^{j+1} \mathbf{u}^*(N-1)$ derived in the previous step to integrate. Calculate the performance index for this segment of the path (i.e. from time $t_f - 3\Delta t$ to t_f). Among the C different values, store the minimum I and the corresponding control as ${}^{j+1} \mathbf{u}^*(N-2)$.

9. Repeat steps 7 and 8 until the initial state is reached (initial condition). Integrate forward along the complete path using all available combinations of control as before and determine the

best one for the initial stage, i.e. ${}^{j+1}\mathbf{u}^*(1)$. This concludes the first iteration. A complete control sequence ${}^{j+1}\mathbf{u}^*(k)$, ($k=1,2,\dots,N$) and an optimal trajectory ${}^{j+1}\mathbf{x}^*(l)$, $l=1,2,\dots,N+1$ are now available for the next iteration.

10. Reduce the size of the control region by setting ${}^{j+1}R = \gamma^j R$. Increase the iteration index j by 1 and repeat the algorithm starting from step 6.

The above algorithm assumes that the whole voyage duration t_f is covered by a wave/swell forecast. If the duration of the voyage exceeds the maximum forecast time, as is the case in the example below, the algorithm needs to be adapted to assume calm water conditions for the segment of the route beyond forecast coverage. In this case, the remaining part of the route will be the great circle arc to the destination point. Figure 12 shows the extent of forecast coverage along the nominal great circle route.

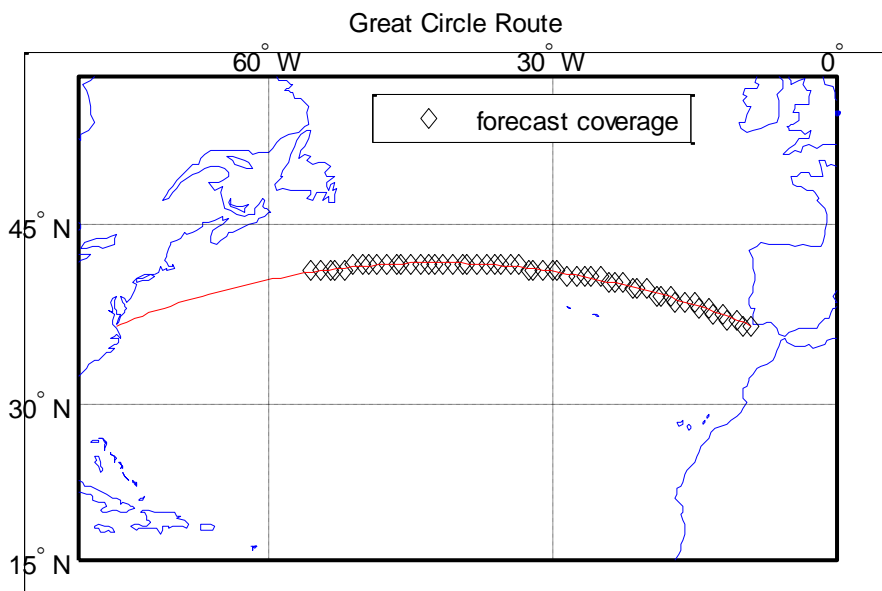


FIGURE 12. Forecast Grid Points Closest to the Great Circle Route.

Assumptions

The length of time stages, as defined in the algorithm above, is chosen to coincide with the forecast interval of 3 hours. Such a short-term description of a sea state allows much confidence in the stationarity assumption discussed earlier. The control policy (i.e. speed and course) is piecewise constant over this time step. No accelerations are taken into account. The transients associated with changing the control input (e.g. engine rpm) are very short relative to the problem's time scale and are neglected. Other components of resistance (such as appendage drag, air resistance, trim or steering resistance) are not included in the analysis. These are either steady components which can be easily incorporated in the model or relatively small in magnitude. The effect of currents is also omitted, as discussed above.

At each stage (time) and for every state (spatial location) the program calculates fuel consumption and checks for constraint violation. For that, it draws information from stored forecast data. In the particular example presented here, the global forecast uploaded on the FTP server of UoA on October 9, 2014 contains the relevant information. For the fraction of the

trip not covered by the forecast calm water is assumed. Ship response and added resistance data are obtained from SWAN1, via the constructed hydrodynamic database, for 10 different speeds (from 7 to 16 knots) and 5 different headings (from 0 to 180 degrees on either side). The actual data are stored in memory in the form of large matrices. Intermediate values are obtained by interpolation. The number of iterations is set to 20 and γ is chosen to be 0.7. The discretization of controls yields a total of $C=50$ combinations of speed and course (5 speed settings and 10 course settings are used in the optimization code).

A longer trip, on the order of several weeks, can be handled by the IDP algorithm as well. In this case, more than one 168-hour forecasts are needed to cover the whole voyage duration. The algorithm is executed at the starting time using the available forecast at that time. The following day, as soon as the next forecast becomes available, the algorithm is executed again with different initial conditions. These are naturally the coordinates of the ship's new position. The final time is also adjusted accordingly. Now the part of the total route not covered by a sea state prediction is shorter. The program is run daily using updated forecasts in a similar fashion until the destination is reached. This process may be executed very efficiently onboard the vessel. It can, in fact, be implemented in short duration voyages as well.

RESULTS AND DISCUSSION

A trans-oceanic passage would normally be planned along the great circle route. In calm seas this is the minimum fuel route, because it is the shortest one. Regardless, the rhumb line route is often considered by the navigator as a reasonable alternative, especially when the great circle routes pass closer to the poles and through more severe seas and/or navigational hazards (e.g. icebergs). Table 4 below presents a comparison of calculation results for the two routes in the numerical example worked out in this text. It can be seen that the loxodrome (rhumb line) is 2.3% longer than the orthodrome (great circle) and about 2.5% more fuel-expensive in calm seas. In rough seas, on the other hand, computation of fuel consumption when sailing the great circle route shows a 45.5% increase in fuel cost compared to the respective calm seas quantity. For the rhumb line route the increase of fuel cost in waves is 14%.

TABLE 4. Great Circle vs. Rhumb Line Routes.

Description	Unit	Value
Great Circle (GC) Distance	naut.miles	3138.6
Rhumb Line (RL) Distance	naut.miles	3210.5
Nominal Voyage Time	days	10.06
Calm Water Speed (GC)	knots	13.0
Calm Water Speed (RL)	knots	13.3
Calm Water Fuel Cost (GC)	tonne	66.89
Calm Water Fuel Cost (RL)	tonne	68.59
Predicted Fuel Cost (GC)	tonne	97.31
Predicted Fuel Cost (RL)	tonne	78.24

Figures 13 to 16 show the fraction of each trajectory in which some safety constraint is violated. In the middle part of the great circle route the WAM forecast predicts wind waves and swell with significant height locally in excess of 9m and 4m respectively. For the rhumb line the predicted figures are about 3.5m and 3m respectively. In both routes the ship encounters these

sea states from head and bow directions. The rhumb line route violates only the deck wetness limiting probability of occurrence.

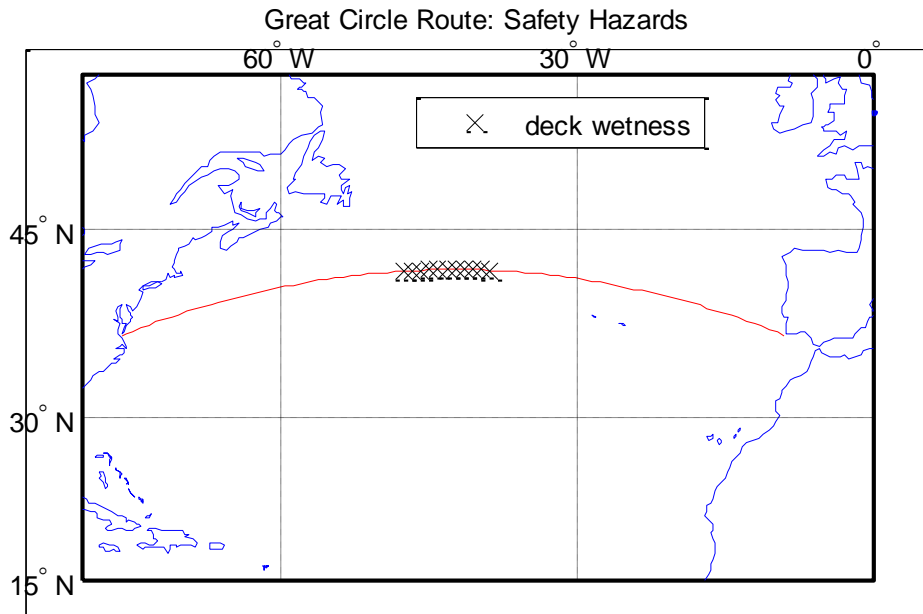


FIGURE 13. Violation of Deck Wetness Constraint along the Orthodrome.

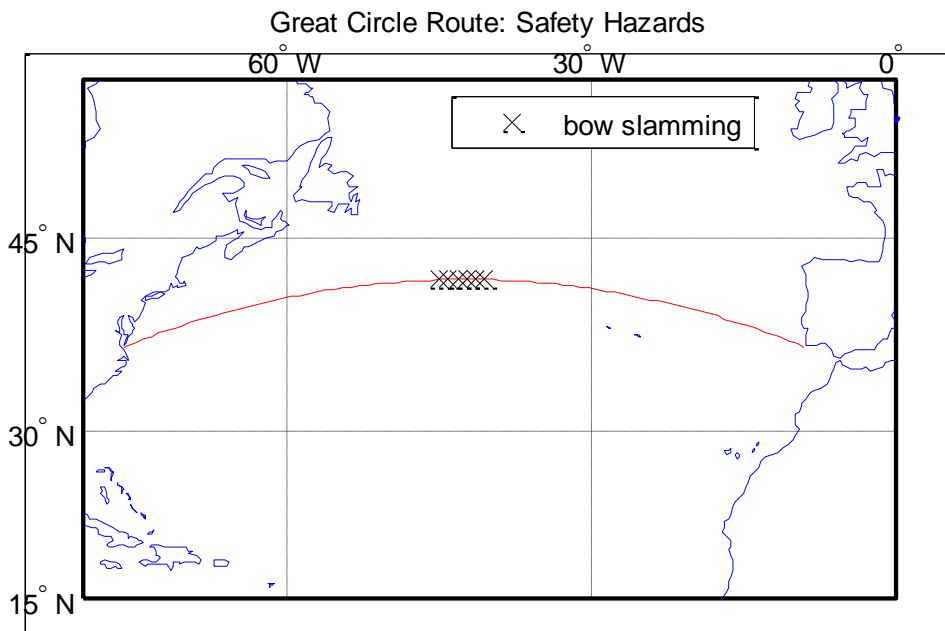


FIGURE 14. Violation of Slamming Constraint along the Orthodrome.

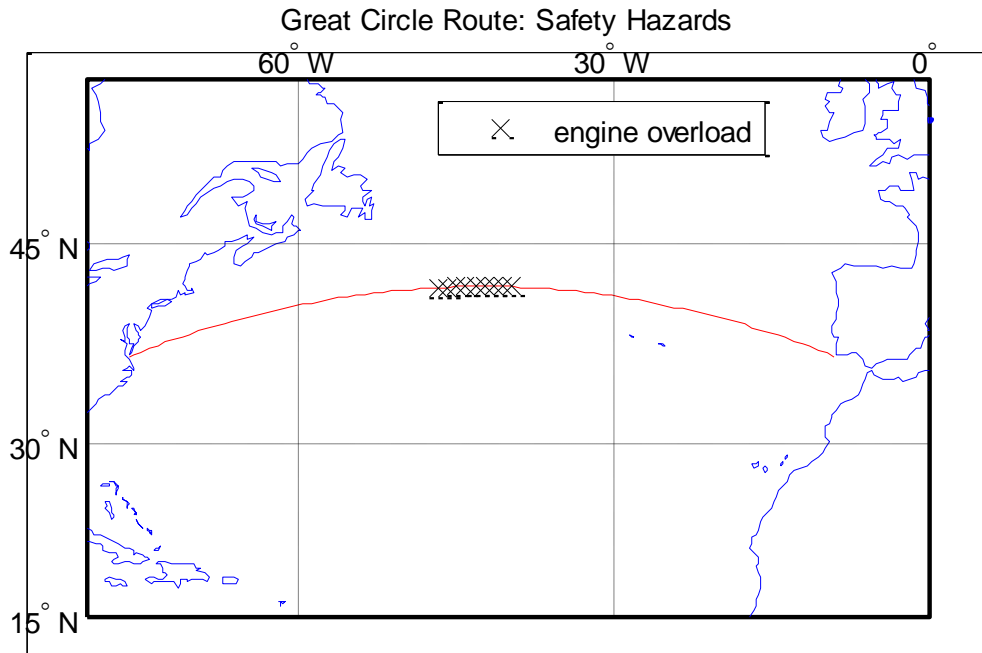


FIGURE 15. Violation of Engine Overload Constraint along the Orthodrome.

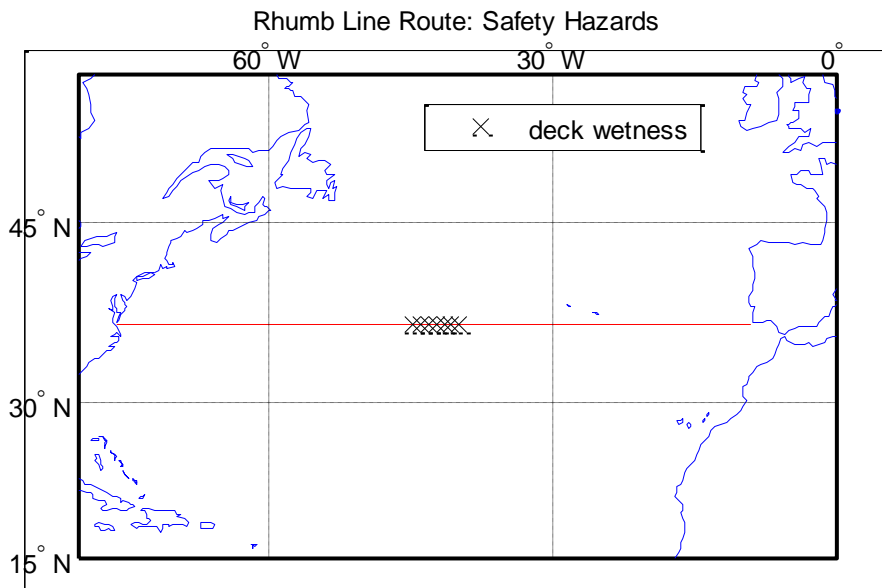


FIGURE 16. Violation of Deck Wetness Constraint along the Loxodrome.

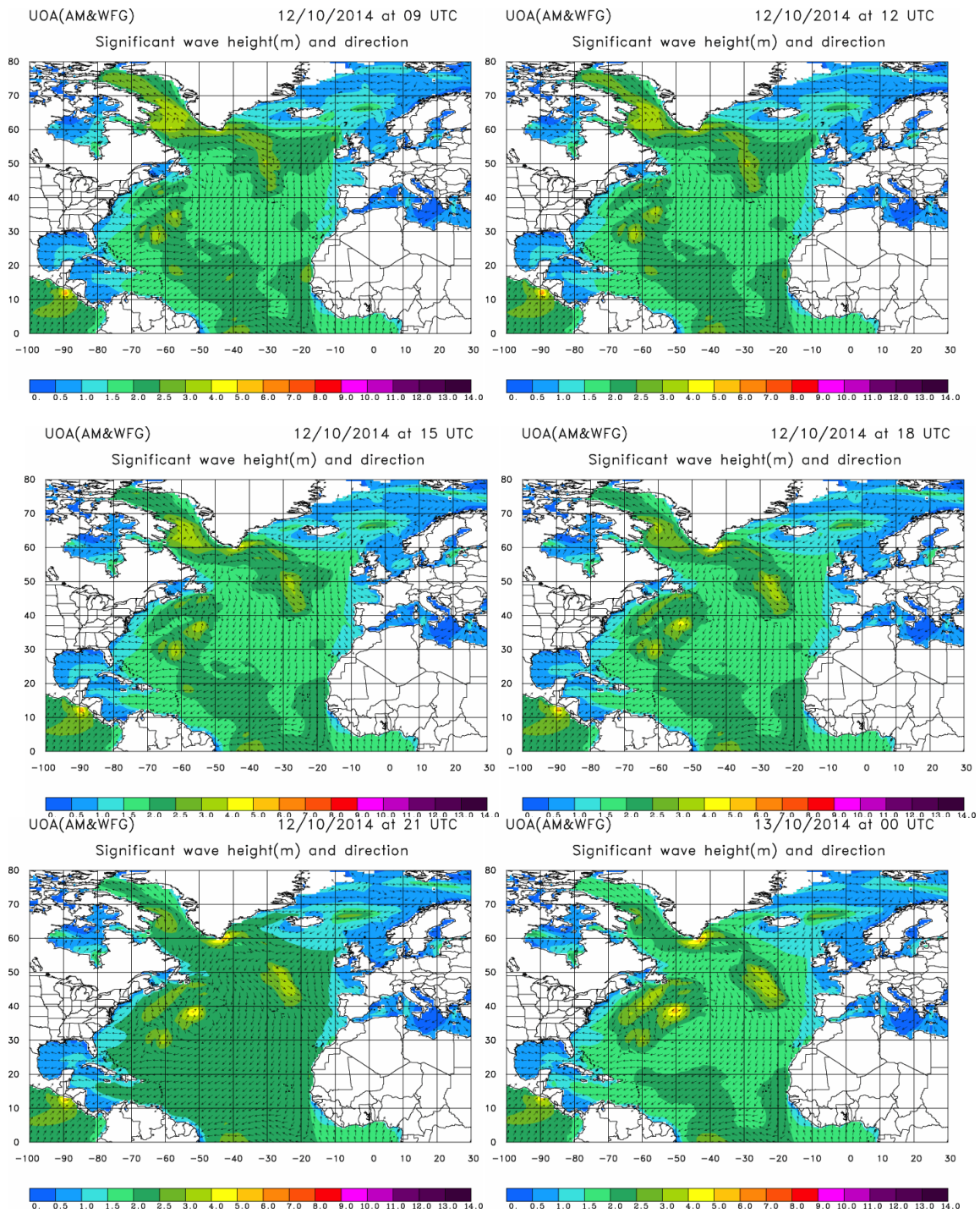


FIGURE 17. Evolution of Wind and Swell Wave System as Forecasted between 105h and 120h of Voyage Time.

The algorithm described in the previous section is coded in MATLAB[®] to generate the fuel minimizing route. First, the code is executed without any constraint considerations. The orthodrome enters the computations as the nominal route (initial guess). The output is depicted in figure 18. The computed optimal route, after 25 iterations, saves 19.8% more bunker fuel than the nominal great circle but only marginally less than the rhumb line (around 0.3%). However,

this route exceeds the specified threshold for deck wetness probability in the portion designated by 'x' marks. This would normally be an infeasible route in the constrained counterpart of the optimization problem, hence it would be ruled out during the code execution. To verify this, the optimization code is run again checking for constraint violation this time. The result is graphically reproduced in figure 19. The optimal control histories for ship's course and speed settings are shown in figures 20 and 21 respectively. Evidently, the optimal route turns sharply towards the north while slowing down at the same time, in order to avoid the high head/bow seas around the middle segment of the trajectory. Then it turns back towards the previous track. After the expiration of the available forecast the gap to the destination point is bridged with a great circle arc.

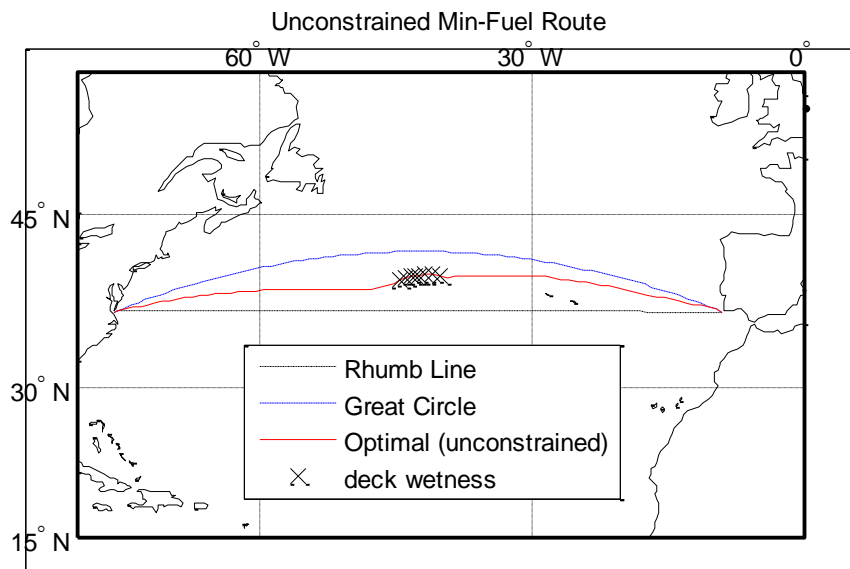


FIGURE 18. Optimal Route of the Unconstrained Minimum Fuel Problem.

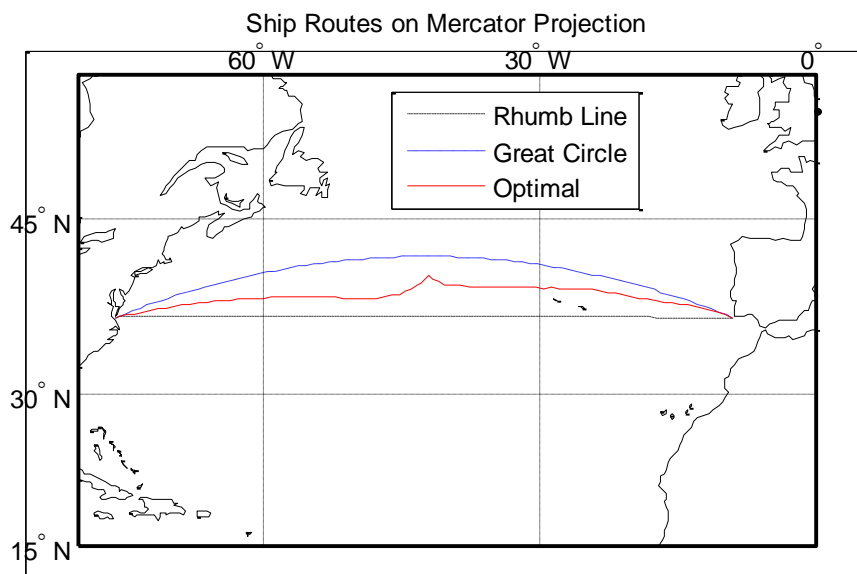


FIGURE 19. Optimal Route of the Constrained Minimum Fuel Problem.

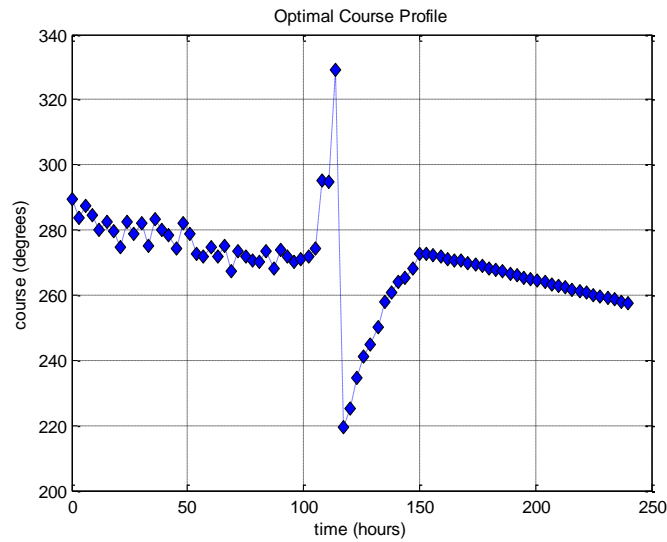


FIGURE 20. Optimal Control History for Ship's Heading.

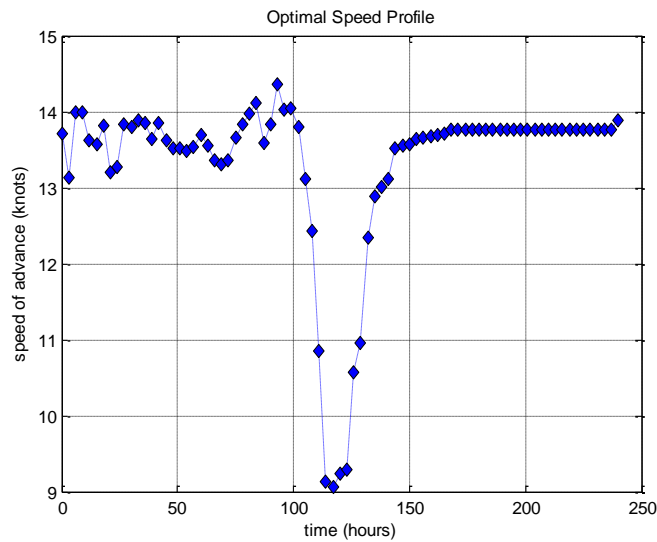


FIGURE 21. Optimal Control History for Ship's Speed.

The structure of the computed optimal solution is intuitive, if one observes the sea state evolution in the mid Atlantic during the voyage of interest (figure 17), bearing in mind that the ship's freeboard is only 2.85m. In this numerical experiment the behavior of the optimal solution is explored under the influence of longitudinal motion-related constraints only. As a result, turning the ship's bow away from the waves both reduces added resistance and alleviates heaving and pitching motions.

Convergence, Accuracy and Sensitivity

Speed of convergence and accuracy are both dominated by the control space C and the contraction factor γ , as defined above in the IDP algorithm. Convergence is illustrated in figure

22 for the constrained optimization problem. To expedite convergence, the optimal solution computed before for the unconstrained problem was used as the initial route in the algorithm. A discussion about tuning the IDP parameters (C , γ , number of iterations) can be found in Avgouleas (2008). The particular optimization scheme with the IDP settings mentioned above was found to be the best compromise between speed of execution and accuracy of the solution.

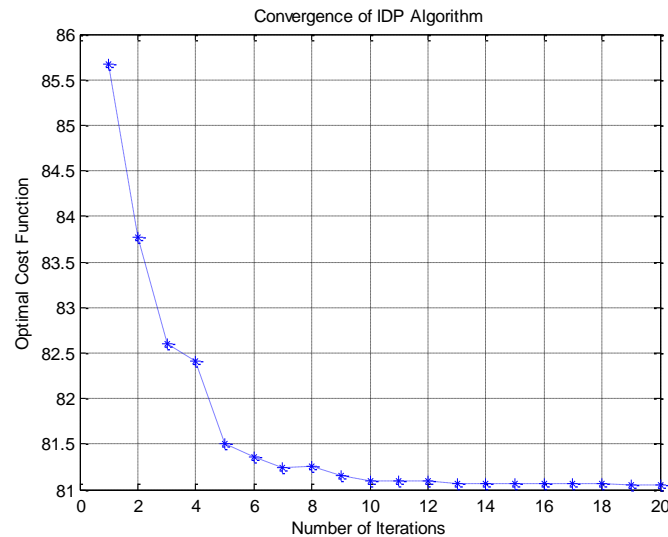


FIGURE 22. Convergence to the Optimal Solution with $\gamma=0.7$.

To assess the sensitivity of the solution to the imposed safety constraints several trials were conducted relaxing or lifting one constraint at a time and then both simultaneously. It is concluded that relaxing the slamming constraint has no effect on the optimal solution. Deck wetness, in contrast, is dominant. In all cases, violation of the slamming constraint occurred together with violation of the deck wetness constraint, but the converse was not true. Altering the limiting value for the probability of occurrence of this event (i.e. green water on deck) changes the structure of the solution significantly. This suggests that the type and limiting values of the constraints must be selected carefully and consistently with the risks that particular vessels and their cargoes encounter in severe sea states. The observed redundancy of the slamming constraint could justify enforcement of a different restriction, such as rolling angle or acceleration. Some caution should be exercised regarding the accuracy of computation of ship motions, if they are to be incorporated as constraints in the program. For example, prescribing a rolling angle (RMS) restriction implies computation of rolling RAOs. If these computations are performed on the basis of ideal flow principles the results may not be realistic, as roll is primarily a viscous phenomenon.

Fuel Savings

There is no simple way to unambiguously quantify the savings in fuel cost in this constrained optimization simulation. The lack of knowledge, in advance, of the navigation track the captain would follow to avoid rough seas makes it difficult to directly compare it to the optimal solution and evaluate its beneficial effect. An estimate may however be obtained by examining feasible routes that satisfy the constraints and comparing them to the optimal.

Any route which brings the ship from the point of departure to the destination point without violating the imposed constraints as well as the voyage final time belongs to the set of feasible routes. The one yielding the lowest value of the assigned performance index (fuel cost, in

particular) is the optimal route. Given the difference in the forecasted severity of the sea between loxodrome and orthodrome, as discussed earlier in this section, existence of a plausible track was investigated to the south of the rhumb line route. This baseline-feasible, sub-optimal route (figure 23) satisfies the prescribed constraints. It was determined by trial and error. Calculation yields a fuel cost of 85.93 tonne for this route. The optimal route of figure 19 requires 5.7% less bunker fuel than the baseline feasible one. Table 5 summarizes the calculated savings. Although the calculated saving rates are heavily dependent on the predicted sea states of the particular example, the benefit of utilizing a decision support system for route selection over sheer intuition or mariner’s experience is indisputable.

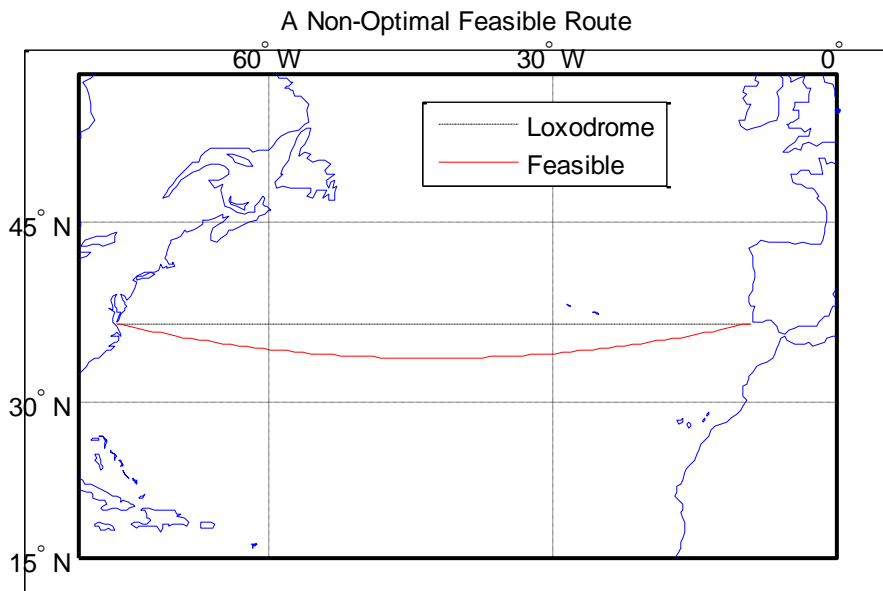


FIGURE. 23. A Baseline Feasible Route South of the Loxodrome.

TABLE 5. Summary of Fuel Savings.

Description	Value
Fuel Cost of Baseline Feasible Route (tonne)	85.93
Fuel Cost of Nominal Route (tonne)	97.31
Fuel Cost of Optimal Route (tonne)	81.06
Fuel Savings Relative to Nominal (%)	16.7
Fuel Savings Relative to Baseline Feasible (%)	5.7

CONCLUSIONS

Fuel-efficient navigation is explored and a solution to the minimum cost routing problem is proposed. An understanding of the governing physics of the problem in question has been emphasized. The dynamics of ship motions and sea state evolution is best captured by state-of-the-art tools like SWAN1 and WAM4. Particular attention should be paid to the added resistance in waves, as it is a driving factor in the vessel routing problem. A comprehensive model for the

optimal control of a ship in waves is developed and a solution has been shown to exist and has been generated using Dynamic Programming. This technique proves to be particularly appealing as it circumvents problematic questions of existence and uniqueness of solution, optimality conditions, existence of derivatives and gradients, all basic requirements of the classical calculus of variations. Furthermore, it is ideally suitable for fast, real time implementation onboard the vessel. Iterative Dynamic Programming, an intelligent alternative to the standard DP algorithm, is found to produce fast results with reasonable accuracy. The main advantage of this alternative, pointed out by Luus (2000) who introduced it, lies in its robustness in obtaining the global optimum. Although there is always a possibility of obtaining a local optimum, careful selection of the IDP parameters usually eliminates this risk and it is proven to give remarkable results in challenging problems, compared to existing well-established methods such as sequential quadratic programming and others. The structure of the optimal solution is strongly affected by the enforced constraints. The findings reveal a great potential in the application of optimal routing methods in shipping. The example-ship used in this paper is a small cargo liner. The magnitude of the derived savings projects to a notable reduction of bunker fuel expenses, especially for tankers, bulk carriers and containerships.

Accurate weather forecasts need to be the subject of a continuous research effort for the results of the present fuel efficient routing algorithm to be significant and useful. The current formulation carries out the optimization of the expected value of the cost function conditioned on a given weather forecast known deterministically. Current weather forecasting technologies allow for the accurate prediction of the expected sea states days in advance. This enables the direct implementation of the optimal ship routing method developed in the present article for the reduction of fuel consumption for trips of the order of weeks by breaking the sailing time into sub-intervals over which the weather forecast is known with a high degree of certainty.

The shipping industry consumes approximately 4 million barrels of oil daily. Assuming that cargo vessels sail into severe sea states approximately 25% of their sailing time, the implementation of the fuel efficient routing algorithm developed in the present study, even using a modest 5% fuel saving rate, would result approximately into a daily reduction of fuel consumption of approximately 50,000 barrels of oil ($=0.25 \times 0.05 \times 4,000,000$). Other than the cost savings by the shipping industry this reduction of crude oil consumption results in a reduction of emissions of CO₂ and other greenhouse gases into the atmosphere. The combined liquid fuels obtained from the refining of an average barrel of oil will produce a minimum of 317kg of CO₂ when consumed. Therefore a reduction of fuel consumption by the shipping industry of 50,000 barrels of oil daily would result in a reduction of 15,850 tonnes of CO₂ emissions. These figures may climb higher under conditions that result in greater fuel savings rates such as the 26% estimated by Tsujimoto and Tanizawa (2006), or the 22.1% estimated by Mezaoui et al. (2009) etc.

The optimal routing methods developed in the present study are readily applicable to the optimal sailing of yachts at the America's Cup level and in open ocean racing. The cost function that must be minimized when sailing a yacht is the time to destination. Weather uncertainty arises from the wind and wave forecasts and accurate forecasts are currently available a day or more in advance. The resistance of sailing yachts in calm water and in a sea state is analogous to that of ships, augmented by the induced drag caused by the wake of the keel, winglets, rudder and sails. The "propulsion" of a sailing yacht arises from the lift force exerted by the wind on the sails. The controls to be optimally selected by the dynamic programming algorithm are the settings of the rudder and trim tabs and the trimming of the sails. Given the advanced state of development of the hydrodynamic and aerodynamic performance attributes of hull forms, appendages and sails the introduction of optimal navigation strategies based on real time dynamic programming methods stands to offer a significant edge in competitive yacht sailing.

A Look Ahead

The model presented in this paper belongs to the broader category of white-box models, namely models fully transparent in the incorporation of the governing physics to the best possible extent. On the other extreme, black-box models exist that are oblivious of the governing physics but rely on real time on-board measurements of relevant parameters to derive the quantities of interest using system identification techniques. The abundance of existing literature makes use of either approach, or combination of both (the so-called “grey-box” models) and claims fuel savings ranging from 2% to over 25%. The savings anticipated by deterministic optimal routing models are unlikely to materialize with the degree of confidence expected by ship owners and operators. The cornerstone of weather routing is wave forecasting. As already mentioned above, the state of the art in wave modeling and forecasting is deterministic, yet the nature of predicting the future sea state is by definition stochastic. Furthermore, variation of a range of parameters would lead to poor prediction of fuel consumption even under the hypothesis of perfect knowledge of future weather. Just to name a few, such parameters could be hull/propeller fouling, engine performance degradation, propeller performance in waves, loading condition, water density, presence of unpredicted currents, bunker fuel heating value and so on. A stochastic optimal weather routing formulation would seek to determine the optimal control strategy which remains optimal under all state variables and uncertainties associated with the problem. This task is challenging in multi-dimensional and stochastic settings and is being addressed as outlined below.

Recent advances in control theory allow the explicit solution of the multi-dimensional stochastic optimal control problem by casting the ship evolution equations in matrix state-space form. In the context of fuel-efficient ship routing the states include: the ship fuel consumption, the propeller RPM, the vessel coordinates relative to an earth-fixed frame, the vessel horizontal velocities, the vessel yaw angle, the vessel yaw rate, the rudder angle, the rudder angular velocity and the parameters discussed in the preceding paragraph. Casting the coupled resistance, maneuvering and seakeeping problems in a multi-dimensional state-space form and allowing for the weather forecasts to be known only stochastically leads to an analytical and efficient determination of the ship route with the minimum fuel consumption using the methods described in Yong and Zhou (1999). The generality and efficiency of this optimal control algorithm would allow its real-time implementation on a ship using a desktop PC. Its implementation to the fuel-efficient ship routing problem is very promising and is the subject of ongoing research.

ACKNOWLEDGMENTS

The contribution of Professor George Kallos from the University of Athens and Professor George Galanis from the Hellenic Naval Academy, Greece, is deeply acknowledged. They provided the output of the WAM4 numerical model for wave and swell forecasting.

REFERENCES

1. Abramowski, Przemyslaw, Tomasz Abramowski, and Zenon Zwierzewicz. 2006. “Formal Solution of Ship Weather Routing Problem via Pontryagin’s Maximum Principle”. *Síntesis Tecnológica*. 3 (1): 27-31.
2. Avgouleas, K. 2008. “Optimal Ship Routing”. SM Thesis, Massachusetts Institute of Technology.
3. Bellman, R.E. 1957. *Dynamic Programming*. Princeton, N.J.: Princeton University Press.
4. Böttner, C. U. 2007. “Weather Routing for Ships in Degraded Condition”. *International Symposium of Maritime Safety, Security and Environmental Protection*, Athens, Greece.

5. Bruns, A., K. Christiansen, and D. Rossow. 2011. "FSG.EcoPilot – an Onboard Tool for Fuel Efficient Speed Profile Selection". In *10th International Conference on Computer and IT Applications in the Maritime Industries (COMPIT'11)*, Berlin, Germany.
6. Delitala, A. M. S., Gallino, S., Villa, L., Lagouvardos, K., Drago, A. 2010. "Weather Routing in Long-Distance Mediterranean Routes". *Theoretical and Applied Climatology* 102 (1-2): 1-2.
7. Dolinskaya, I. S., M. Kotinis, M. G. Parsons, and R. L. Smith. 2009. "Optimal Short-Range Routing of Vessels in a Seaway". *Journal of Ship Research*, Society of Naval Architects and Marine Engineers 53 (3): 121-9.
8. Dolinskaya, Irina S. 2012. "Optimal Path Finding in Direction, Location, and Time Dependent Environments". *Naval Research Logistics (NRL)* 59 (5): 325-39.
9. Emmanouil, G., G. Galanis, and G. Kallos. 2007. "Assimilation of Radar Altimeter Data in Numerical Wave Models: an Impact Study in Two Different Wave Climate Regions". *Annales Geophysicae*, 25(3): p. 581-596.
10. Faltinsen, O.M., K. J. Minsaas, N. Liapis, and S. O. Skørddal. 1980. "Prediction of Resistance and Propulsion of a Ship in a Seaway". In *13th Symposium on Naval Hydrodynamics*. T. Inui. Editor. The Shipbuilding Research Association of Japan: Tokyo. p. 505-530.
11. Faltinsen, O.M. 1990. *Sea Loads on Ships and Offshore Structures*. Cambridge Ocean Technology Series, 1, Cambridge; New York: Cambridge University Press.
12. Gerritsma, J., and W. Beukelman. 1972. "Analysis of the Resistance in Waves of a Fast Cargo Ship". *International Shipbuilding Progress*, 19(217): p. 285-293.
13. Gershanik V.I. 2011. "Weather Routing Optimisation - Challenges and Rewards. Proceedings of the Institute of Marine Engineering, Science and Technology Part A: *Journal of Marine Engineering and Technology*. 10 (3): 29-40.
14. Hinnenthal, J., and G. Clauss,. 2010. "Robust Pareto-Optimum Routing of Ships Utilising Deterministic and Ensemble Weather Forecasts". *Ships and Offshore Structures* 5 (2): 105-14.
15. Hotrop, J. 1984. "A Statistical Re-Analysis of Resistance and Propulsion Data". *International Shipbuilding Progress*, 31(363): p. 272-276.
16. Illus, T., and A. Heikkinen. 2012. "Challenges in Vessel Speed Optimization". In *11th International Conference on Computer and IT Applications in the Maritime Industries (COMPIT'12)*, Liege, Belgium.
17. Kirk, D.E. 1970. *Optimal Control Theory: an Introduction*. Englewood Cliffs, N.J.: Prentice-Hall.
18. Kobayashi, E., T. Asajima, and N. Sueyoshi. 2011. "Advanced Navigation Route Optimization for an Oceangoing Vessel". In *Methods and Algorithms in Navigation – Marine Navigation and Safety of Sea Transportation*, eds. Adam Weintrit, Tomasz Neumann, 149-155CRC Press.
19. Kosmas, O. T., and D. S. Vlachos. 2012. "Simulated Annealing for Optimal Ship Routing". *Computers & Operations Research* 39 (3) (3): 576-81.
20. Krata, P., and J. Szlapczynska. 2011. "Weather Hazard Avoidance in Modeling Safety of Motor-Driven Ship for Multicriteria Weather Routing". In *Methods and Algorithms in Navigation – Marine Navigation and Safety of Sea Transportation*, eds. Adam Weintrit, Tomasz Neumann, 165-172CRC Press.
21. Luus, R. 2000. *Iterative Dynamic Programming*. Boca Raton: Chapman & Hall/CRC.
22. MAK 9M25C Project Guide –Propulsion, Issue July 2008, Caterpillar Motoren GmbH & Co. KG, (downloaded from www.stet.pt).
23. Maki, Atsuo, Youhei Akimoto, Yuichi Nagata, Shigenobu Kobayashi, Eiichi Kobayashi, Shigeaki Shiotani, Teruo Ohsawa, and Naoya Umeda. 2011. "A New Weather-Routing System that Accounts for Ship Stability Based on a Real-Coded Genetic Algorithm". *Journal of Marine Science and Technology* 16, (3) (09): 311-322.
24. Marie, S., and E. Courteille. 2009. "Multi-Objective Optimization of Motor Vessel Route". In *Marine Navigation and Safety of Sea Transportation*, ed. Adam Weintrit, 411-418CRC Press.
25. Marie, S., and E. Courteille. 2014. "Sail-Assisted Motor Vessels Weather Routing Using a Fuzzy Logic Model". *Journal of Marine Science and Technology* 19: 265-279.
26. Mezaoui, B., K. Takashima, and R. Shoji. 2009. "On the Fuel Saving Operation for Coastal Merchant Ships Using Weather Routing". In *Marine Navigation and Safety of Sea Transportation*, ed. Adam Weintrit, 431-436CRC Press.
27. Montes, A. 2005. "Network Shortest Path Application for Optimum Track Ship Routing". MSc thesis, Naval Postgraduate School.
28. Ochi, M.K. 1998. *Ocean Waves: the Stochastic Approach*. Cambridge Ocean Technology Series, 6, Cambridge, U.K.; New York: Cambridge University Press.

29. Sen D. and Padhy C.P. 2009. "Development of a Ship Weather Routing Algorithm and its Application for Indian Coastal Sea Routes". *International Journal of Ecology and Development* 12 (W09): 59-74.
30. Panigrahi, J. K., Padhy, C. P., Sen, D., Swain, J., Larsen, O. 2012. "Optimal Ship Tracking on a Navigation Route between Two Ports: A Hydrodynamics Approach". *Journal of Marine Science and Technology* 17 (1): 59-67.
31. Panigrahi, J. K., Tripathy, J. K., Umesh, P.A.,. 2008. "Optimum Tracking of Ship Routes in 3g-WAM Simulated Rough Weather Using IRS-P4 (MSMR) Analysed Wind Fields". *Journal of the Indian Society of Remote Sensing* 36 (2): 149-58.
32. Pipchenko, O. 2011. "On the Method of Ship's Transoceanic Route Planning". In *Methods and Algorithms in Navigation – Marine Navigation and Safety of Sea Transportation*. eds. Adam Weintrit, Tomasz Neumann, 157-163CRC Press.
33. Rathe, H., and C. Beiersdorf. 2005. "Decision Support for Container Ship Operation in Heavy Seas – Shipboard Routing Assistance" In *4th International Conference on Computer and IT Applications in the Maritime Industries (COMPIT'05)*, Hamburg, Germany.
34. Sclavounos, P.D., and D.E.Nakos. 1993. "Seakeeping and Added Resistance of I.A.C.C. Yachts by Three-Dimensional Rankine Panel Methods". In *11th Chesapeake Sailing Yacht Symposium*. Annapolis MD.
35. Shao W., Zhou P., Thong S.K. 2012. "Development of a Novel Forward Dynamic Programming Method for Weather Routing". *Journal of Marine Science and Technology (Japan)* 17 (2): 239-51.
36. Skoglund, L., J. Kutteneuler, and A. Rosén. 2012. "A New Method for Robust Route Optimization in Ensemble Weather Forecasts". *Trita-AVE / KTH Aeronautical and Vehicle Engineering* 2012:67 .
37. Szłapczyńska, J. 2007. "Multiobjective Approach to Weather Routing". *Advances in Marine Navigation and Safety of Sea Transportation*. Proceedings of TransNav 2007, Gdynia 2007. Gdynia Maritime University.
38. Szłapczyńska, J. 2013. "Multicriteria Evolutionary Weather Routing Algorithm in Practice". *International Journal on Marine Navigation and Safety of Sea Transportation*, TransNav 7 (1): 61-5.
39. Szłapczyńska, J., and R. Smierzchalski. 2007. "Adapted Isochrone Method Improving Ship Safety in Weather Routing with Evolutionary Approach". *International Journal of Reliability, Quality and Safety Engineering*. 14 (06): 635-645.
40. Szłapczyńska, J., and R. Smierzchalski. 2009. "Multicriteria Optimisation in Weather Routing". In *Marine Navigation and Safety of Sea Transportation*, ed. Adam Weintrit, 423-429CRC Press.
41. Todd, F.H. 1963. "Series 60 Methodical Experiments with Models of Single-Screw Merchant Ships". Washington: For sale by the Supt. of Docs., U.S. Govt. Print. Off.
42. Tsou, Ming-Cheng and Hung-Chih Cheng. 2013. "An Ant Colony Algorithm for Efficient Ship Routing". *Polish Maritime Research*. 20(3): 3-50
43. Tsujimoto, M., and K. Tanizawa. 2006. "Development of a Weather Adaptive Navigation System Considering Ship Performance". In *Actual Seas, 25th International Conference on Offshore Mechanics and Arctic Engineering*, Proceedings of OMAE 2006, Germany.
44. Wisniewski, B., J. Chomski, and P. Medyna. 2009. "Application of the 1-2-3 Rule for Calculations of a Vessel's Route Using Evolutionary Algorithms". In *Marine Navigation and Safety of Sea Transportation*, ed. Adam Weintrit, 419-422CRC Press.
45. Yong, J. and X. Z. Zhou. 1999. *Stochastic Controls: Hamiltonian Systems and HJB Equations*. Applications of Mathematics Series, 43, Springer-Verlag, New York.